circulator including those of the adjusting elements and the electromagnet is about 1 m in length and 0.5 m in height, and the total weight is 120 kg.

IV. Conclusion

A 30-kW CW waveguide Y-junction circulator at 915 MHz has been realized with protruding metal cylinders into the waveguide junction, with thin ferrite disks on their flat surfaces. On the basis of this result, a 100-kW CW waveguide Y-junction circulator was developed by inserting three additional metal disks within the junction region, and by attaching ferrite disks on each surface of the water-cooled metal disks. Each ferrite disk is water-cooled efficiently and the input power to the circulator is divided equally by a multilayer structure.

The design of a 100-kW CW waveguide Y-junction circulator at 915 MHz was obtained by analyzing the relationship between the ferrite dimensions and the air-gap considering power dissipation in the ferrite. The dimensions of the ferrite disk and the air-gap were determined very easily, and the utility of this design technique was confirmed experimentally. It was found that the internal dc magnetic-field distribution influences the performance of the circulator.

This approach was found to be very important for designing high-power circulators which require low insertion loss. The 30-kW and 100-kW Y-junction circulators have good performance, are compact and can be built economically. The results indicate that a 100-kW CW waveguide Y-junction circulator at 2450 MHz and at other frequencies can be realized by using this type of configuration.

Acknowledgment

The authors wish to thank M. Mori and M. Yasuda of Tokyo Denshi Giken Corporation, for their great assistance in performing the experiments, and also H. Takahashi of Nippon Microwave Company for providing some of the ferrite samples.

References

[1] Y. Konishi, "A high-power circulator," *IEEE Trans. Microwave Theory Tech.*, vol. MTT-15, pp. 700–708, Dec. 1967.
[2] F. Okada, K. Ohwi, and M. Mori, "The development of a high-power microwave circulator for use in breaking of concrete and rock," *J. Microwave Power*, vol. 10, pp. 171–180, Feb. 1975.
[3] F. Okada, K. Ohwi, and M. Mori, "A 100 kW waveguide circulator with multi-layer ferrite disks at 915 MHz," in *Proc. 1977 IMPI Symp.*, paper 4B-6, July 1977.
[4] N. Tsukamoto, M. Suzuki, and T. Matsumoto, "An analysis of the waveguide Y-junction with ferrite," *I.E.C.E. Japan, Trans.*, vol. 54-B, pp. 131–138, Apr. 1971.
[5] H. Takamizawa *et al.*, "CaVBi garnets with linewidths narrowed by means of a hot-pressing process," in *Powder and Powder Metallurgical Society, 1972 Annual Convention Rec., Japan*, no. 2-17, Nov. 1972.
[6] H. Takamizawa *et al.*, "Polycrystalline calcium–vanadium garnets with narrow ferrimagnetic resonance," *IEEE Trans. Magnetics*, vol. MAG-8, pp. 446–449, Apr. 1972.
[7] C. E. Fay and R. L. Comstock, "Operation of the ferrite junction circulator," *IEEE Trans. Microwave Theory Tech.*, vol. MTT-13, pp. 15–27, Jan. 1965.
[8] J. Helszajn and F. C. Tan, "Design data for radial-waveguide circulators using partial-height ferrite resonators," *IEEE Trans. Microwave Theory Tech.*, vol. MTT-23, pp. 288–298, Mar. 1975.
[9] B. Lax and K. J. Button, *Microwave Ferrite and Ferimagnetics*. New York: McGraw-Hill, 1962.
[10] J. R. Eshbach, "Spin-wave propagation and the magnetoelastic interaction in yttrium iron garnet," *J. Appl. Phys.*, vol. 34, pp. 1298–1304, Apr. 1963.
[11] B. Owen, "The identification of modal resonances in ferrite loaded waveguide Y-junctions and their adjustment for circulation," *Bell Syst. Tech. J.*, vol. 51, pp. 595–627, Mar. 1972.

Generation of Microwave Power with a Spark-Gap Cavity

VELIMIR M. RISTIC, MEMBER, IEEE, AND THOMAS P. SORENSEN

***Abstract*—A theory of a $\lambda/4$ transmission line resonator containing a spark gap is developed and parameters such as output spectrum, bandwidth, Q factor, and efficiency are derived. Equivalent circuits incorporating different spark-gap parameters are presented and used for numerical simulation of cavity output. Several fixed and variable frequency cavities are constructed and tested. Typical peak power outputs are 7.2 kW into 50-Ω line at a frequency of 2.1 GHz, and 27 kW into 50-Ω line at a frequency of 1.5 GHz. For proper operation of this device the spark resistance must fall to a value less than the characteristic impedance of the line in a time less than T where $f_0 = 1/2T$ is the required frequency.**

Manuscript received May 10, 1977; revised October 15, 1977.
The authors are with the Department of Electrical Engineering, University of Toronto, Toronto, Ont. M5S 1A4, Canada.

I. Introduction

SPARK GAP switches are well known as they have been used in radar equipment for many years as

0018-9480/78/0500-0369$00.75

transmit-receive (T-R) switches, and more recently in devices such as travatron [1], frozen-wave generators [2], baseband radar systems [3], and pulsed laser systems [4]. In this paper, we develop a theory of a $\lambda/4$ transmission line resonator with a spark gap as a means for exciting the resonator. The emphasis is in using such a cavity for the generation of high peak-power RF bursts in the frequency range from 0.2 to 3 GHz. It is shown that by appropriate modeling of the spark gap the parameters and the output power of the cavity are predictable. For proper operation of these devices the spark resistance must fall to a value less than the characteristic impedance of the line in a time less than T where $f_0 = 1/2T$ is the required frequency.

II. Theory of Transmission Line Resonator

Consider the transmission line shown in Fig. 1. In the first analysis it is assumed that the spark is a perfect switch with zero formative time and a constant resistance R_0. It is also assumed that the switch (i.e., spark gap) is physically very close to the partial short position and the partial short is approximated by a perfect short.

Let V_0 be the voltage on the transmission line when the switch is closed at time $t=0$. The magnitude of the reflected voltage V_R which travels towards the open circuit is given by $V_R = V_0 Z_0/(R_0+Z_0)$ where Z_0 is the characteristic impedance of the line, and the current flowing through the resistor is given by $I_R = V_0/(R_0+Z_0)$. The wave traveling down the line is reflected without change of voltage sign at the open circuit and reaches the resistor again at time $t=2L/v=T$, where L is the length of the line and v the velocity of propagation along the line. Following the analysis by Lewis and Wells [5], it can be shown that, at the output, the ratio of the second voltage peak which occurs when $T \leqslant t \leqslant 2T$ to the first peak at $0 \leqslant t \leqslant T$ is given by

$$-\frac{2Z_0}{R_0+Z_0} \tag{1}$$

and that the ratio of any other voltage peak to the preceding peak is given by

$$\frac{V(NT \leqslant t < (N+1)T)}{V((N-1)T \leqslant t \leqslant NT)} = \frac{R_0 - Z_0}{R_0 + Z_0}. \tag{2}$$

The spark is assumed to have a finite rise time less than T with a wavefront $c(t)$, where $c(t)=0$ for $t<0$, $c(t)=1$ for $t \geqslant T$ where $0 \leqslant c(t) < 1$ represents the wavefront for $0 \leqslant t \leqslant T$. Setting $b(t)=c'(t)$, we have $b(t)=c'(t)$ for $0 \leqslant t \leqslant T$, and $b(t)=0$ for all other values of t.

The coupling is assumed small if the resulting coupling resistance is small in respect to spark-gap resistance R_0. If $V(f)$ is the Fourier transform of the output voltage $v(t)$ then the output power spectrum, $P(f)$ is equal to $|V(f)|^2/Z_1$ where Z_1 is the characteristic impedance of the output transmission line, as shown in Fig. 1.

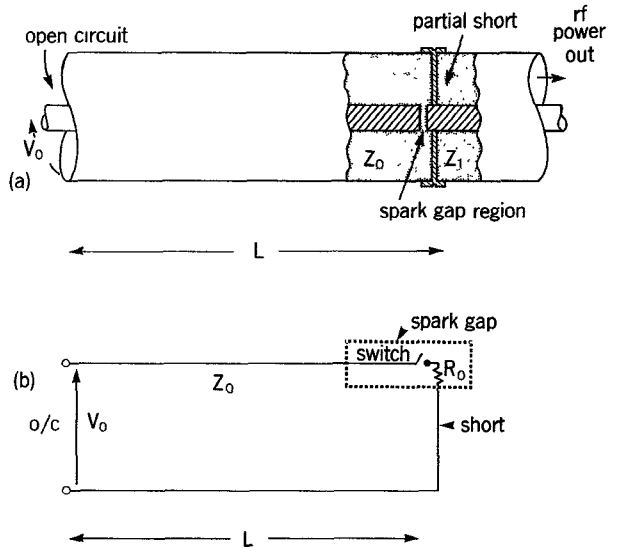

Fig. 1. Schematic (a) and equivalent representation (b) of the transmission line resonator; Z_0 and Z_1 are the characteristic impedances of the resonator and output transmission lines, respectively, R_0 is the spark-gap (switch) resistance, and L is the length of the resonator. The cross-hatched radial line in (a) indicates a partial short.

The resulting power spectrum $P(f)$ is given by

$$P(f) = \frac{K^2 V_0^2 |B(f)|^2}{Z_1 Z_0^2} P_1(R,f) \tag{3}$$

where K is a constant representing the coupling. Furthermore,

$$P_1(R,f) = \frac{1}{R^2+1}\left(\frac{1-\cos 2\pi f t}{1-\left((R^2-1)/(R^2+1)\right)\cos 2\pi f T}\right) \tag{4}$$

where $B(f)$ is the Fourier transform of $b(t)$ and $R = R_0/Z_0$ is the normalized spark resistance. The 3-dB bandwidth and the Q factor of the system can be determined from (4) for $R \ll 1$. If the fundamental frequency is denoted by $f_0 = 1/2T$ and the 3-dB point frequency by f_b, the half-power bandwidth is given by

$$\Delta f = 2(f_b - f_0) = \frac{4R}{\pi} f_0 \tag{5}$$

and the resulting Q factor is

$$Q_0 = \frac{f_0}{[2(f_b - f_0)]} = \frac{\pi}{4R}. \tag{6}$$

In order to calculate the effect of rise time on the magnitude and shape of the output spectrum it was assumed that

$$c(t) = \begin{cases} \frac{1}{2}(1-\cos(\pi t a/T)), & \text{for } 0 \phi t \leqslant T/a \\ 0, & \text{for } t<0 \\ 1, & \text{for } t \geqslant T/a \end{cases} \tag{7}$$

where $a \geqslant 1$. It was established that if the rise time was halved, i.e., a change from 1 to 2, the power at the fundamental frequency was increased by a factor of 1.43. The partial short may be considered more accurately as a

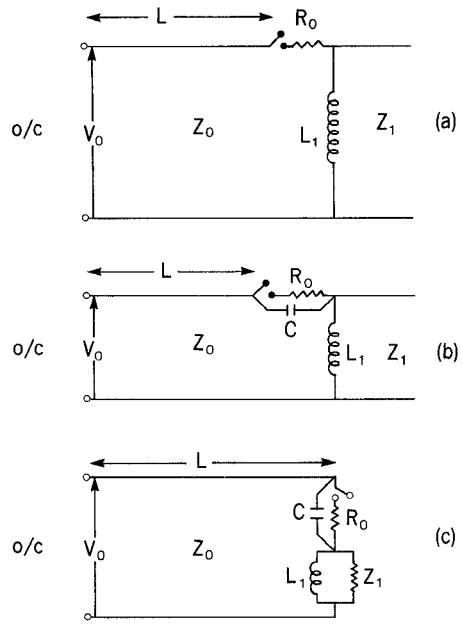

Fig. 2. Equivalent circuits for the cavity: (a) with coupling inductance L_1; (b) with coupling inductance and spark-gap capacitance C; and (c) with coupling inductance, spark-gap capacitance, and loading Z_1.

small inductance, L_1 across the transmission line so that the system may be more accurately represented as shown in Fig. 2(a). This is another step in a more realistic modeling of the device. The voltage across the output transmission line is then given by $L_1(dI/dt)$. Substituting L_1 for K in (3) the maximum peak power at fundamental frequency for any "a" is then given by

$$P_{\max}=\frac{64L_1^2V_0^2f_0^2}{Z_1Z_0^2(R+1)^4}\left(\frac{\cos(\pi/2)a}{1-(1/a)^2}\right)^2. \tag{8}$$

The efficiency of coupling, E can be defined as the ratio of the maximum peak power divided by the product of the fundamental frequency and the initial energy stored in the length L of the transmission line, and is given by

$$E=\frac{512L_1^2f_0^2}{Z_1Z_0(R+1)^4}\frac{\cos(\pi/2)a}{1-(1/a)^2}. \tag{9}$$

Up to this point it has been assumed that the coupling was small enough so as not to affect the resonant circuit. In order to make the system more efficient, however, large coupling is required. The effect of strong coupling mechanism on the resonant circuit will now be considered.

A. Theory of Transmission Line Resonator for Arbitrary Inductive Post Coupling Including Spark-Gap Capacitance Effects.

Consider a transmission line shown in Fig. 2(b) where it is assumed that the spark is a perfect switch with zero formative time and that it has a constant resistance R_0. The spark-gap capacitance C shown is the interelectrode capacitance and is given by $C=\epsilon_0A/d$, where A is the area of the face of the electrodes and d the interelectrode spacing. It is also assumed that the switch (i.e., spark gap) is very close (compared to line length) to the partial short position. The partial short may be represented by an inductance L_1 across the output transmission line of characteristic impedance Z_1. Fig. 2(c) shows the equivalent circuit of this system with indicated voltage and currents. Solving the transmission line equations in real time and then using Fourier transform we obtain the expression for the output power spectrum

$$P(f)=\frac{L_1^2V_0^2}{Z_0^2Z_1}\frac{(1-\cos 2\pi ft)}{H(f)} \tag{10}$$

where

$$H(f)=\left\{\left(-\omega^2L_1CR+R\right)^2+\left(\frac{\omega L_1}{Z_1}R+\frac{\omega L_1}{Z_0}\right)^2\right\}\cdot\{1-\cos 2\pi fT\}$$
$$+2\left\{\omega RR_0C\left(1-\omega^2L_1C\right)-\omega L_1\left(\frac{1}{Z_0}-\frac{\omega^2L_1CRR_0}{Z_1^2}\right)\right\}\cdot\sin 2\pi fT$$
$$+\left(1+\frac{\omega^2L_1^2}{Z_1^2}\right)(1+\omega^2C^2R_0^2)(1+\cos 2\pi fT). \tag{11}$$

The maxima of the output power spectrum, under the assumptions of $\omega L_1/Z_1\ll 1$, $\omega L_1/Z_0\ll 1$, $\omega CR_0\ll 1$, and $\omega CRR_0\ll 1$ occur at frequencies

$$\omega_n=N\omega_0\left\{1+\left(RR_0C-\frac{L_1}{Z_0}\right)\frac{2}{\pi}\omega_0\right\} \tag{12}$$

where $N=1,3,5,\cdots$ is the harmonic number and ω_n are the new resonant frequencies. The effects of coupling when the spark-gap capacitance is neglected can be investigated using (10) with $C=0$. For $R\ll 1$ and $Q\gg 1$, the Q factor of the nth-order maxima is given by

$$Q_n=\frac{\pi N}{4\left(R+\omega_n^2L_1^2/Z_0Z_1\right)}=\frac{\pi N}{4\left(R+N^2\omega_1^2L_1^2/Z_0Z_1\right)}. \tag{13}$$

Thus we see that for small values of coupling and normalized spark resistance, the effect of the coupling on the resonator may be represented by a frequency shift given by (12) with $C=0$ and an increased normalized resistance given by

$$R_T=R+\frac{N^2\omega_1^2L_1^2}{Z_0Z_1}. \tag{14}$$

Moreover, it is seen from (13) when coupling effects are comparable to spark losses, the bandwidth increases for the higher harmonics. Equation (13) may now be used to separate the coupling spark resistance effects if the bandwidth of the fundamental and of any other harmonic are

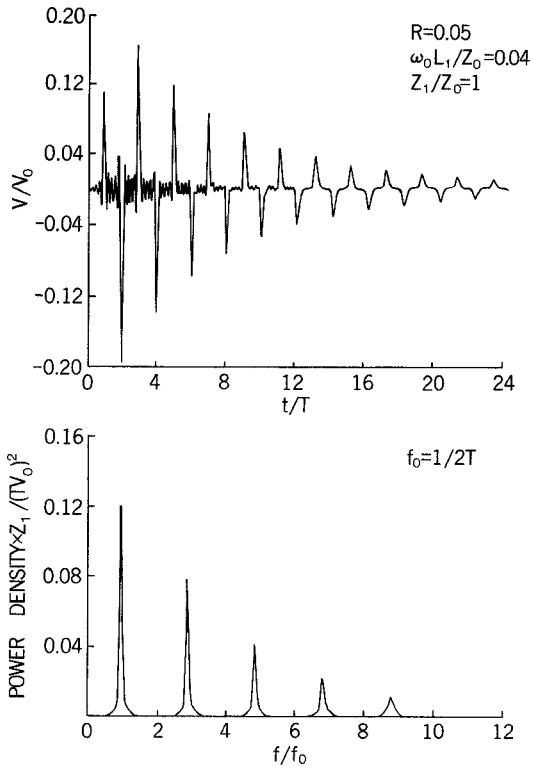

Fig. 3. Normalized time and frequency response of the output voltage ($R=0.5$, $\omega_0 L_1/Z_0=0.04$, $Z_1/Z_0=1$).

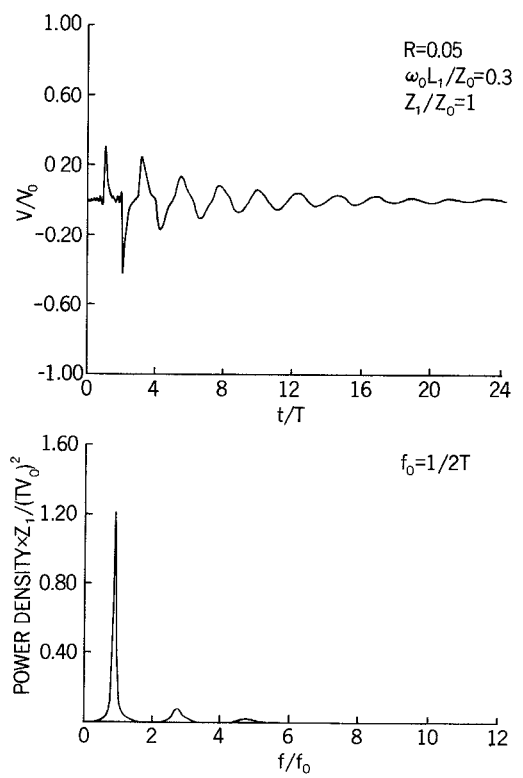

Fig. 4. Normalized time and frequency response of the output voltage ($R=0.05$, $\omega_0 L_1/Z_0=0.3$, $Z_1/Z_0=1.0$).

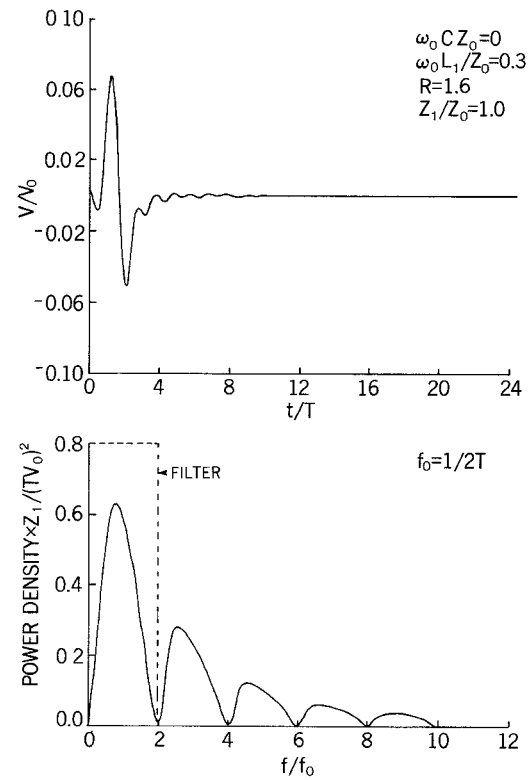

Fig. 5. Normalized time response from filtered frequency response ($\omega_0 CZ_0=0$, $\omega_0 L_1/Z_0=0.3$, $R=1.6$, $Z_1/Z_0=1.0$).

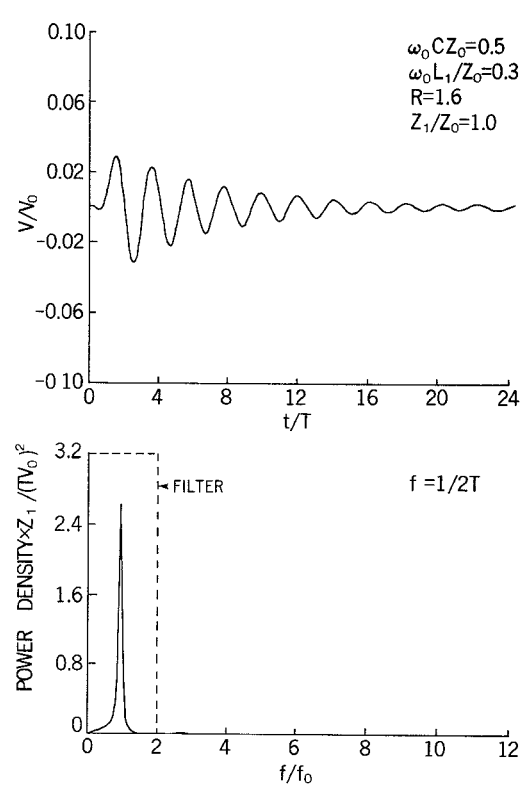

Fig. 6. Normalized time response from filtered frequency response ($\omega_0 CZ=5$, $\omega_0 L_1/Z_0=0.3$, $R=1.6$, $Z_1/Z_0=1.0$).

measured. We obtain the following results:

$$\frac{\omega_1^2 L_1^2}{Z_0 Z_1} = \frac{\pi}{4Q_1}\left(\frac{(B_n/B_1)-1}{N^2-1}\right) \tag{15}$$

and

$$R = \frac{\pi}{4Q_1}\left(\frac{N^2-(B_n/B_1)}{N^2-1}\right) \tag{16}$$

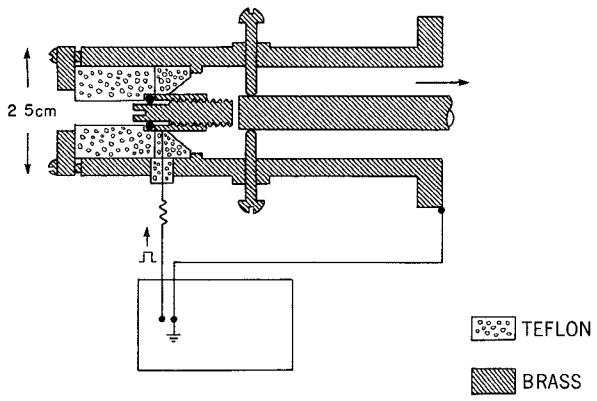

Fig. 7. Cross-section of the fixed frequency device.

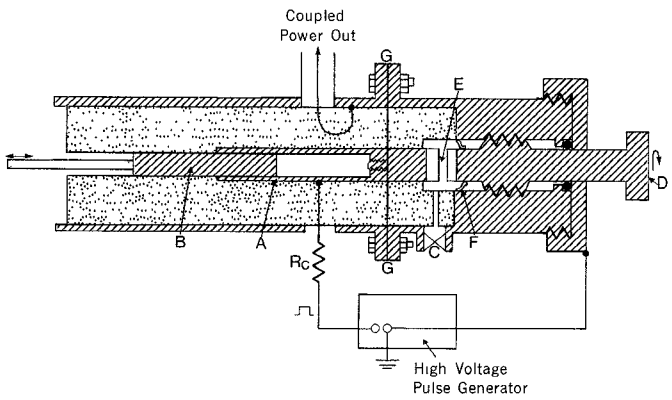

Fig. 8. Construction of the variable frequency device. The isolating resistor R_c can be replaced with $\lambda/4$ stub to increase efficiency.

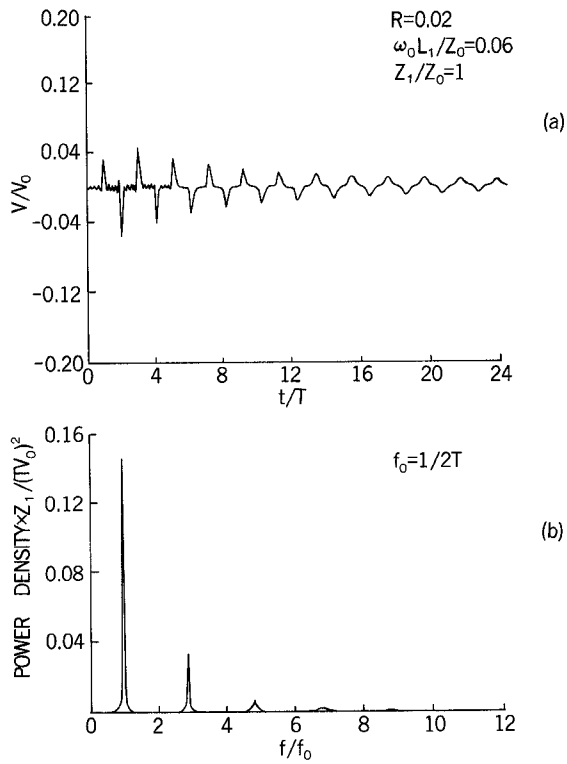

Fig. 9. Normalized output voltage (a) and power density (b) of the cavity versus normalized time and frequency, respectively. These outputs should be compared with the experimental results shown in Fig. 10.

where B_n is the bandwidth of the Nth harmonic and Q_1 is the Q of the fundamental.

It is seen that the effective coupling impedance is proportional to L_1^2/Z_0Z_1 whereas the frequency shift due to the partial short coupling is proportional to L_1/Z_0. Thus to maximize the coupling and minimize the frequency shift we must have $Z_1 \ll Z_0$.

In order to obtain the time response of $v_2(t)$ a digital computer was employed, using a fact Fourier transform algorithm to calculate the inverse Fourier transform of the output voltages. Only frequencies up to and including the nineth harmonic were used in calculating the time response. The program can easily be adapted to filter the response and thus, for example, plot only the fundamental harmonic, if peak power at only the fundamental harmonic is of interest.

Figs. 3 and 4 demonstrate the computer output for varying values of $\omega_0 L_0/Z_0$ with $Z_0/Z_1 = 1$ and $R = 0.05$. The value of C has been set to zero in these plots as we wish to examine only the coupling effects. It may be shown that when neglecting effects of the coupling mechanism, the Q factor is given by

$$Q_n \approx \frac{\pi N}{4R\left(1-\frac{1}{2}\omega_n^2 R_0^2 C^2\right)} = \frac{\pi N}{4R\left(1-\frac{1}{2}N^2\omega_1^2 R_0^2 C^2\right)}. \quad (17)$$

Thus we see that for $\omega_n CRR_0 \ll 1$ and $\omega_n CRR_0 \ll 1$ the effect of gap capacitance on the resonator may be represented by a frequency shift given by (12) with $L_1 = 0$ and a decreased normalized resistance given by

$$R_T = R\left(1-\tfrac{1}{2}N^2\omega_1^2 R_0^2 C^2\right). \quad (18)$$

The effect of gap capacitance therefore is to decrease the bandwidth of the output spectrum and increase the peak spectral level. These results for small values of $\omega_1 R_0 C$ would indicate that the gap capacitance might possibly be employed to obtain a limited bandwidth output when the normalized spark gap resistance is large. Figs. 5 and 6 show the theoretical spectral and time responses as the capacitance of the gap is increased. Only frequencies less than $2f_0$ are used in evaluating the time response. In each case the normalized spark resistance R is set equal to 1.6.

III. Experimental Investigation

Several fixed and variable frequency cavities were constructed [6] and tested with air, N, He, and SF_6, at pressures up to 200 lb/in^2. The cross-sections of the devices are shown in Figs. 7 and 8. The modeling of the spark gap was successful as indicated by the numerical output, Fig. 9 and the experimental data, Fig. 10. Typical peak power outputs are 7.2 kW into 50-Ω line at a

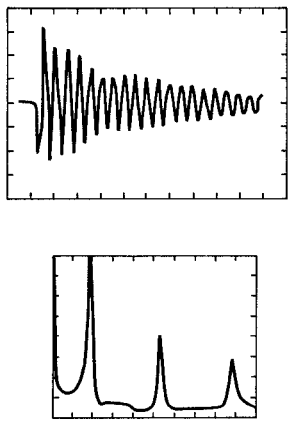

Fig. 10. Output voltage of the cavity. (a) Time response, horizontal scale 10 ns/cm, vertical scale 200 mV/cm with 60-dB attenuation in the line; (b) Spectral response, horizontal scale 100 MHz/cm (0–1 GHz coverage), vertical scale linear.

frequency of 2.1 GHz and 27 kW into 50 Ω at a frequency of 1.5 GHz. The rise times were on the order of 200 ps. Using the available data [7] for normalized spark-gap resistance it was concluded that operation of the device at X band is feasible.

IV. Conclusions

For proper operation of this device at frequencies less than 3 GHz the spark resistance must fall to a value less than the characteristic impedance of the line in a time less than T where $f_0 = 1/2T$ is the required frequency. The faster the rise time the more efficient is the operation of this device.

If a partial short is used, for minimal frequency shift due to coupling, the largest possible ratio of Z_0/Z_1 (where Z_0 is the characteristic impedance of the line and Z_1 is the characteristic impedance of the output transmission line) should be used, and the inductance L_1 should be adjusted for the required coupling. At low frequencies when the cross-sectional dimensions are limited it may not be possible to make L_1 large enough to give the required coupling. In this case it will be necessary to decrease Z_0 in order to increase the coupling. The decrease of Z_0/Z_1 will result in a decrease of the resonant frequency. At frequencies higher than 3 GHz the spark-gap capacitance may be used to give a limited bandwidth output even though the normalized spark resistance, R is less than unity.

Acknowledgment

The authors acknowledge the support from Defense Research Establishment Ottawa and National Research Council of Canada.

References

[1] J. M. Proud, Jr., and W. H. McNeill, "High power travatron investigation," RADC-TR-74-33, AD777881.
[2] S. D. Houston, and D. Bailey, "Hertzian generator development," RADC-TR-73-325, AD774567.
[3] G. F. Ross, "A balanced antenna-generator for the distortionless radiation of subnanosecond pulses," in *1971 G-AP Int. Symp. Dig.*, pp. 311–314, Sept. 1971.
[4] L. S. Levine and I. M. Vitkovitsky, "Pulsed power technology for controlled thermonuclear fusion," *IEEE Trans. Nuclear Sci., vol. NS-18*, pp. 255–264, Aug. 1971.
[5] I. A. D. Lewis and F. H. Wells, *Millimicrosecond Pulse Techniques* New York, McGraw-Hill, 1959.
[6] V. M. Ristic and T. P. Sorensen, "Plasma excited microwave cavity," Canadian Patent Office Registration No. 918 343, 1975.
[7] T. P. Sorensen and V. M. Ristic "Rise time and time-dependent spark-gap resistance in nitrogen and helium," *J. Appl. Phys.*, vol. 48, pp. 114–117, Jan. 1977.

Correction to "Behavior of the Magnetostatic Wave in a Periodically Corrugated YIG Slab"

MAKOTO TSUTSUMI, MEMBER, IEEE, YASUNORI SAKAGUCHI, AND NOBUAKI KUMAGAI, SENIOR MEMBER, IEEE

In the above short paper,[1] in (21) the minus sign was inadvertently left out. Equation (21) should read as follows:

$$-B_{z0}\cos\hat{\theta}+B_{x0}\sin\hat{\theta}=-B_z\cos\hat{\theta}+B_x\sin\hat{\theta}.$$

Consequently, the following correction should be noted.

1) In the second and seventh lines of (23) substitute $+(\pi/d)\Delta$ and $+(K_z+(2\pi/d)m)$ for $-(\pi/d)\Delta$ and $-(K_z+(2\pi/d)m)$, respectively;

2) In (24) and (27), the factor $[1-((\pi/d)\Delta)^2]$ and $[\mu_1-((\pi/d)\Delta)^2]$ should have read $[1+((\pi/d)\Delta)^2]$ and $[\mu_1+((\pi/d)\Delta)^2]$, respectively.

Since the numerical computation was based on the assumption that $1\gg((\pi/d)\Delta)^2$ and $\mu_1\gg((\pi/d)\Delta)^2$, the results and conclusions reported in the paper are unaffected by this revision.

Manuscript received March 20, 1978.
The authors are with the Department of Electrical Communication Engineering, Osaka University, Suita, Osaka 565, Japan.
[1] M. Tsutsumi, Y. Sakaguchi, and N. Kumagai, *IEEE Trans. Microwave Theory Tech.*, vol. MTT-25, pp. 224–228, Mar. 1977.